

# Quark spectral properties above $T_c$ from Dyson-Schwinger equations

Jens A. Mueller,<sup>1</sup> Christian S. Fischer,<sup>1,2,3</sup> and Dominik Nickel<sup>4</sup>

<sup>1</sup>*Institut für Kernphysik, Technische Universität Darmstadt, Schlossgartenstraße 9,  
D-64289 Darmstadt, Germany*

<sup>2</sup>*Institut für Theoretische Physik, Universität Giessen, 35392 Giessen, Germany*

<sup>3</sup>*GSI Helmholtzzentrum für Schwerionenforschung GmbH, Planckstr. 1 D-64291 Darmstadt, Germany.*

<sup>4</sup>*Institute for Nuclear Theory, University of Washington, Seattle, WA 98195*

(Dated: October 31, 2018)

We report on an analysis of the quark spectral representation at finite temperatures based on the quark propagator determined from its Dyson-Schwinger equation in Landau gauge. In Euclidean space we achieve nice agreement with recent results from quenched lattice QCD. We find different analytical properties of the quark propagator below and above the deconfinement transition. Using a variety of ansätze for the spectral function we then analyze the possible quasiparticle spectrum, in particular its quark mass and momentum dependence in the high temperature phase. This analysis is completed by an application of the Maximum Entropy Method, in principle allowing for any positive semi-definite spectral function. Our results motivate a more direct determination of the spectral function in the framework of Dyson-Schwinger equations.

PACS numbers: 12.38.Mh, 14.65.Bt, 25.75.Nq

## I. INTRODUCTION

The wealth of data produced by the Relativistic Heavy-Ion Collider (RHIC) has led to new insights about the nature of the quark-gluon plasma (QGP), in particular in the strongly coupled regime just above the chiral phase transition (see Refs. [1–4] for recent reviews). Despite the strong coupling, phenomena like the constituent quark number scaling of elliptic flow [5] still suggest quarks as quasiparticle excitations. This should also be connected with the success of quasiparticle models in describing thermodynamic properties in this regime of the QCD phase diagram [6, 7] and also serves as a foundation for transport approaches like the one discussed in Ref. [8]. In another context, dilepton production in a heavy ion collision has been related to the spectral properties of the thermalized quasiparticles and specifically to the dispersion relation of quarks [9–11]. We therefore conclude that a detailed understanding of the quasiparticle spectrum, in particular close to the chiral phase transition, is desirable.

Our quantity of interest is the quark spectral function, which encodes all information about the two-point correlation function, in particular also its poles and consequently the quark’s dispersion relation and decay width. In the realm of weak coupling reliable results are obtained using the hard-thermal loop (HTL) expansion [12–14]: One finds the by now well-known pattern of two quasiparticle excitations and a continuum contribution stemming from a branch cut in the quark propagator due to Landau damping, i.e. the absorption of a space-like quark by a hard gluon or hard antiquark. The two quasiparticles correspond to an ordinary quark with a positive ratio of chirality to helicity and to a collective mode dubbed ‘plasmino’ with a negative chirality to helicity ratio. Both have thermal masses of order  $gT$  and decay widths of order  $g^2T$ , where  $g$  is the coupling constant and  $T$  the

temperature.

Beyond systematic weak-coupling expansions, there is no straightforward approach for the determination of the spectral function or its characteristics. Some insight has been gained using model calculations, finding similar structures as in the weak coupling limit besides a possible additional third quasiparticle excitation which is only present at small momenta [15–17]. The width of the quasiparticle peaks, which is of order  $g^2T$  in HTL approximation, might however become of the order of the thermal mass for couplings at the scale of the chiral phase transition [18]. This questions the existence of well-defined quasiparticles at least at small momenta.

Ab initio calculations of correlators within lattice QCD are performed in Euclidean space and an analytic continuation that is necessary to determine the spectral function is strictly speaking not possible. There are, however, approaches that aim to extract attributes of spectral functions from the numerical data. One of these is the Maximum Entropy Method (MEM) [19, 20], which has been applied in similar contexts, e.g. for extracting the spectral functions of mesons [21, 22]. For cold and dense matter MEM has also been applied within the framework of Dyson-Schwinger equations (DSEs) in Ref. [23]. In some sense MEM corresponds to fitting the “most likely” spectral function to the data but without restricting the form of the spectral function. In contrast to this another method has been established in Refs. [24, 25]. There the authors assumed a certain shape for the quark spectral function including a few fitting parameters which were determined from the numerical data. In such an approach one relies on physical guidance as e.g. given by the HTL approximation for the construction of a suitable ansatz for the spectral function.

A complementary approach to the correlators of QCD are functional methods such as Dyson-Schwinger equations and the functional renormalisation group. In re-

cent years, these methods have been successfully applied to problems such as the characterization of the chiral and deconfinement transition [26–32], or the properties of gluons in the high temperature phase [33–35]. In this work we do the first steps towards the determination of spectral functions in the framework of Dyson-Schwinger equations beyond simple rainbow approximations. Particularly due to our input for the gluon propagator the DSE calculations are also limited to Euclidean space and we use the two methods described above to explore the possible shape of the spectral function. The truncation scheme is detailed in section II and has been shown to reproduce the chiral and deconfinement transition temperatures of quenched lattice QCD in Ref. [32]. In section III we briefly present our results for the quark dressing functions in Euclidean space below and above the critical temperature  $T_c$ . We then introduce the spectral representation for the quark propagator in section IV. Using fit ansätze for the spectral function, we focus on zero momentum and finite quark masses in section V before moving to finite momentum in the chirally restored phase in section VI. The obtained results are confronted with recent quenched lattice QCD results from Ref. [25]. Finally we evaluate our truncation scheme using MEM in section VII, before we conclude in section VIII and outline possible future directions.

## II. QUARK DYSON-SCHWINGER EQUATION AND EMPLOYED TRUNCATIONS

### A. Quark Dyson-Schwinger equation

The renormalized quark Dyson-Schwinger equation in the Matsubara formalism is given by

$$S^{-1}(i\omega_p, \mathbf{p}) = Z_2 S_0^{-1}(i\omega_p, \mathbf{p}) - \Sigma(i\omega_p, \mathbf{p}), \quad (1)$$

with the inverse full quark propagator  $S^{-1}(i\omega_p, \mathbf{p})$ , the quark wave function renormalization constant  $Z_2$ , the inverse bare quark propagator  $S_0^{-1}(i\omega_p, \mathbf{p})$  and the to-be-specified self-energy  $\Sigma(i\omega_p, \mathbf{p})$ . With the only difference of explicitly using imaginary arguments for the energy in all functions, we follow the conventions from Ref. [32]. For the fermionic Matsubara frequencies we have  $\omega_p = (2n_p + 1)\pi T$  with temperature  $T$ . For the Dirac structure of the inverse propagators we have

$$S_0^{-1}(i\omega_p, \mathbf{p}) = i\gamma_4 \omega_p + i\boldsymbol{\gamma} \cdot \mathbf{p} + Z_m m(\mu), \quad (2)$$

$$S^{-1}(i\omega_p, \mathbf{p}) = i\gamma_4 \omega_p C(i\omega_p, |\mathbf{p}|) + i\boldsymbol{\gamma} \cdot \mathbf{p} A(i\omega_p, |\mathbf{p}|) + B(i\omega_p, |\mathbf{p}|), \quad (3)$$

i.e. the inverse full propagator is parameterized by the dressing functions  $A(i\omega_p, |\mathbf{p}|)$ ,  $B(i\omega_p, |\mathbf{p}|)$  and  $C(i\omega_p, |\mathbf{p}|)$ . The quark mass renormalization constant  $Z_m$  and the renormalized mass  $m(\mu^2)$  at renormalization scale  $\mu$ , together with  $Z_2$ , are then determined within a MOM-renormalization scheme.

In Landau gauge, the self-energy takes the form

$$\begin{aligned} \Sigma(i\omega_p, \mathbf{p}) = & \frac{16\pi}{3} \frac{Z_2}{Z_3} \alpha(\mu) T \sum_{n_q} \int \frac{d^3 q}{(2\pi)^3} \left[ \gamma_\mu S(i\omega_q, \mathbf{q}) \right. \\ & \left. \times \Gamma_\nu(i\omega_q, \mathbf{q}, i\omega_p, \mathbf{p}) D_{\mu\nu}(i\omega_p - i\omega_q, \mathbf{p} - \mathbf{q}) \right], \end{aligned} \quad (4)$$

with gluon propagator  $D_{\mu\nu}$ , quark-gluon vertex  $\Gamma_\nu$ , gauge coupling  $\alpha(\mu)$  and ghost renormalization constant  $Z_3$ . Assuming we know  $D_{\mu\nu}$ ,  $\Gamma_\nu$  and the renormalization procedure, the DSE then translates into coupled nonlinear integral equations for the desired dressing functions.

### B. Truncation setup

The gluon propagator being a major ingredient in the quark DSE, can in principle be obtained in quenched approximation from corresponding DSE's [33–36]. However, this turns out to be a formidable task and the results are still on a qualitative level only. We therefore use results from lattice gauge theory as input. These have been made available recently on a fine temperature grid over a temperature range from 0 to  $2.2 T_c$  [32].

In Landau gauge the gluon propagator is given through transverse and longitudinal dressing functions  $Z_T(i\tilde{\omega}_k, |\mathbf{k}|)$  and  $Z_L(i\tilde{\omega}_k, |\mathbf{k}|)$ , respectively, via

$$D_{\mu\nu}(i\tilde{\omega}_k, \mathbf{k}) = \frac{Z_T(i\tilde{\omega}_k, |\mathbf{k}|)}{k^2} P_{\mu\nu}^T(k) + \frac{Z_L(i\tilde{\omega}_k, |\mathbf{k}|)}{k^2} P_{\mu\nu}^L(k). \quad (5)$$

Hereby we introduced the projectors

$$\begin{aligned} P_{\mu\nu}^T(k) &= (1 - \delta_{\mu 4})(1 - \delta_{\nu 4}) \left( \delta_{\mu\nu} - \frac{k_\mu k_\nu}{k^2} \right), \\ P_{\mu\nu}^L(k) &= \delta_{\mu\nu} - \frac{k_\mu k_\nu}{k^2} - P_{\mu\nu}^T(k), \end{aligned} \quad (6)$$

the bosonic Matsubara frequency  $\tilde{\omega}_k = 2\pi n_k T$  and the short-hand notation  $k_\mu = (\tilde{\omega}_k, \mathbf{k})_\mu$ , for which  $k^2 = \tilde{\omega}_k^2 + \mathbf{k}^2$ . As in the case of quark propagator and quark-gluon vertex we suppress color indices due to the remaining global color symmetry.

The gluon dressing functions,  $Z_T$  and  $Z_L$ , have been calculated in quenched lattice gauge theory for gauge group SU(2) and SU(3) [32]. In the quark Dyson-Schwinger equation we also need to evaluate the gluon propagator for momenta not identically to the ones of the lattice calculation. Therefore we use temperature dependent fits to these data. In Fig. 1 we show results for gauge group SU(3) which is the relevant gauge group in this work. The figure presents the lattice results denoted by data points together with corresponding fit functions represented by straight lines for a variety of temperatures. The explicit expressions for the fit functions and

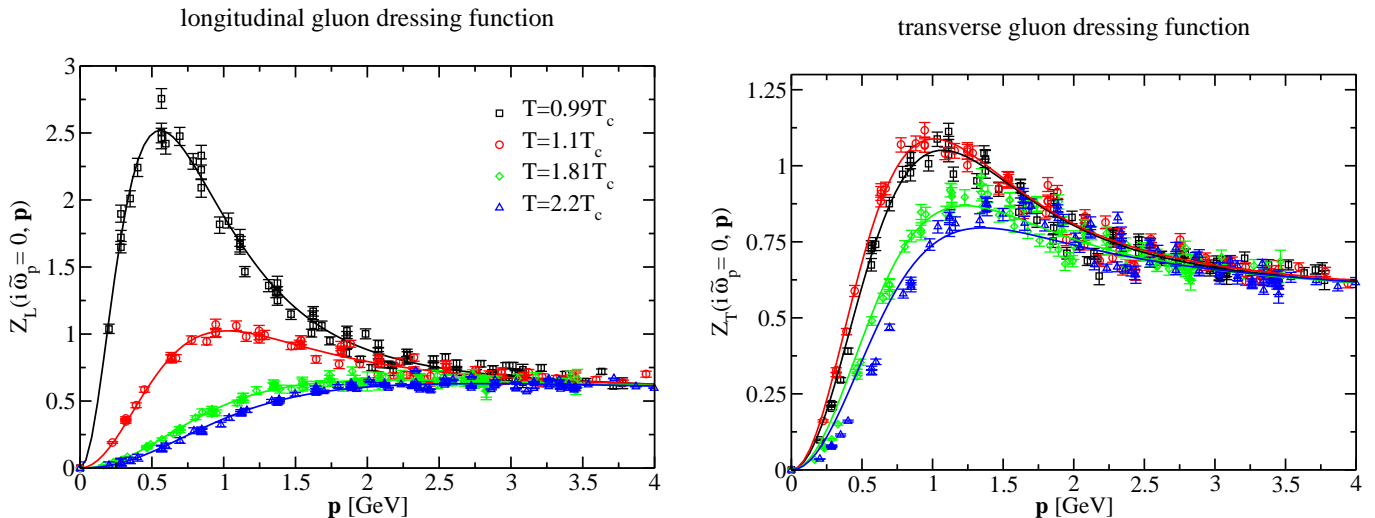


FIG. 1: Longitudinal (left) and transverse (right) temperature dependent gluon dressing function for the lowest Matsubara frequency from lattice calculations compared with our fits. Shown are results for temperatures below the critical temperature ( $0.99 T_c$ ) and above the critical temperature ( $1.1 T_c$ ,  $1.81 T_c$ ,  $2.2 T_c$ ).

a more detailed discussion concerning the gluon propagator can be found in Ref. [32] and shall not be repeated here for brevity.

The details of the second ingredient for a closed quark DSE, namely the quark-gluon vertex, are yet to be explored. First exploratory results on the mass and momentum dependence of the vertex at zero temperature have been reported from lattice calculations and Dyson-Schwinger equations, see [37, 38] and Refs. therein. How-

ever, not much is known about its temperature dependence. In such a situation a viable strategy is to use phenomenological model ansätze for the vertex which are then justified by comparing results with other approaches. This strategy has been successful in previous works [32] and will therefore also be adopted here.

In the following we employ the temperature dependent ansatz for the vertex used in Refs. [29, 30, 32]. It is given by

$$\Gamma_\nu(i\omega_q, \mathbf{q}, i\omega_p, \mathbf{p}) = \tilde{Z}_3 \left( \delta_{4\nu}\gamma_4 \frac{C(i\omega_q, |\mathbf{q}|) + C(i\omega_p, |\mathbf{p}|)}{2} + (1 - \delta_{4\nu})\gamma_\nu \frac{A(i\omega_q, |\mathbf{q}|) + A(i\omega_p, |\mathbf{p}|)}{2} \right) \times \left( \frac{d_1}{d_2 + k^2} + \frac{k^2}{\Lambda^2 + k^2} \left( \frac{\beta_0 \alpha(\mu) \ln[k^2/\Lambda^2 + 1]}{4\pi} \right)^{2\delta} \right), \quad (7)$$

with the gluon momentum  $k_\mu = (\omega_p - \omega_q, \mathbf{p} - \mathbf{q})_\mu$  and  $\beta_0 = 11$  for quenched QCD. The anomalous dimension of the vertex  $\delta$  accounts for the correct perturbative running coupling. It is given by  $\delta = -9/44$  and we renormalize at  $\alpha(\mu) = 0.3$ . The Dirac structure with the quark vector dressing functions  $A$ ,  $C$  represents the first component of the Ball-Chiu vertex at finite temperature. It is motivated by the Slavnov-Taylor identity for the vertex and constitutes a first approach towards a more realistic non-trivial temperature dependence of the vertex. In the additional phenomenological fit function we have parameters  $d_1$  and  $d_2$  and the temperature independent scale  $\Lambda = 1.4$  GeV. Since we use lattice results as reference for the gluon propagator, the quark-gluon vertex is the

only uncertainty source in our calculation. We adjust the parameter  $d_1$  temperature dependent while keeping  $d_2 = 0.5$  GeV<sup>2</sup> independent of temperature. As for  $d_1$  it turns out that its temperature dependence is in one-to-one correlation to the thermal masses  $m_T$  of the quarks as extracted in section V. Since the same quantity has been determined from quenched QCD results for the Landau gauge quark propagator, see Tab. II of Ref. [25], we adjust  $d_1$  such that it roughly coincides with these results. This procedure works only above the critical temperature where thermal masses can be extracted. Below the critical temperature no such information is available and we therefore choose the constant value  $d_1 = 4.6$  GeV<sup>2</sup>. This choice ensures spontaneous chiral symmetry break-

ing and agrees with the one used in Ref. [32]. We certainly checked the  $d_1$  dependence of our results for the quark spectral function below the critical temperatures; this is discussed in section V. Our values of  $d_1$  and the obtained thermal masses are summarized in Tab. I. Obviously, the strength of the vertex ansatz at low momenta is significantly reduced above the critical temperature. This is what one may expect: In the Dyson-Schwinger equation for the quark-gluon vertex, discussed in detail in Ref. [38], we find skeleton diagrams containing dressed gluon propagators. As is evident from Fig. 1 there is a rapid decrease in the strength of the longitudinal gluon at or around the critical temperature  $T_c$ . This rapid decrease will backfeed into the vertex DSE which probably explains the reduction of the strength of the quark-gluon vertex. This behavior fits nicely to our findings for the parameter  $d_1$  in our ansatz for the vertex. We therefore believe that our vertex ansatz accurately reflects qualitative and maybe even quantitative features of the fully dressed quark-gluon vertex.

### III. MATSUBARA PROPAGATOR BELOW AND ABOVE $T_c$

Before we focus on the spectral functions we briefly discuss our results for the Matsubara propagator in momentum space shown in Fig. 2. The results are obtained employing a sharp cutoff  $\Lambda$  for the computation of the self-energy. Thus the integration and summation extends to momenta and frequencies with  $\omega_q^2 + \mathbf{q}^2 \leq \Lambda^2$ . For  $|n_q| \leq 39$  the summation over Matsubara frequencies is performed explicitly. The remaining sum is approximated by an integral and we checked that the results are insensitive to a change of the number of explicitly summed Matsubara modes. We then use a MOM-renormalization scheme with renormalization conditions  $C(i\omega_0, \boldsymbol{\mu}) = 1$  and  $B(i\omega_0, \boldsymbol{\mu}) = m(\boldsymbol{\mu})$  and  $\omega_0^2 + \boldsymbol{\mu}^2 = 10545 \text{ GeV}^2$ ; consequently all dressing functions are independent of the cutoff  $\Lambda$ . More details concerning the numerical procedure can be found in Ref. [30].

In Fig. 2 we show results for  $m(\boldsymbol{\mu}) = 25 \text{ MeV}$ . Above  $T_c$  the interaction strength as parameterized by the quark-gluon vertex is strongly reduced and the dressing functions  $A(i\omega_0, \mathbf{p})$  and  $C(i\omega_0, \mathbf{p})$ , which are finite in Landau gauge, do not deviate much from unity. In the infrared all dressing functions are constant and we observe that  $A(i\omega_0, \mathbf{p}) < C(i\omega_0, \mathbf{p})$ . This is also found for the dressing functions in HTL approximation [39], where this inequality holds for all momenta. In the simplified case

TABLE I: Temperature dependent parameter for the quark-gluon vertex and extracted thermal masses  $m_T$ .

$T/T_c$	$< 1$	1.25	1.5	2.2
$d_1 [\text{GeV}^2]$	4.6	0.5	0.4	0.25
$m_T/T$		0.865	0.862	0.822

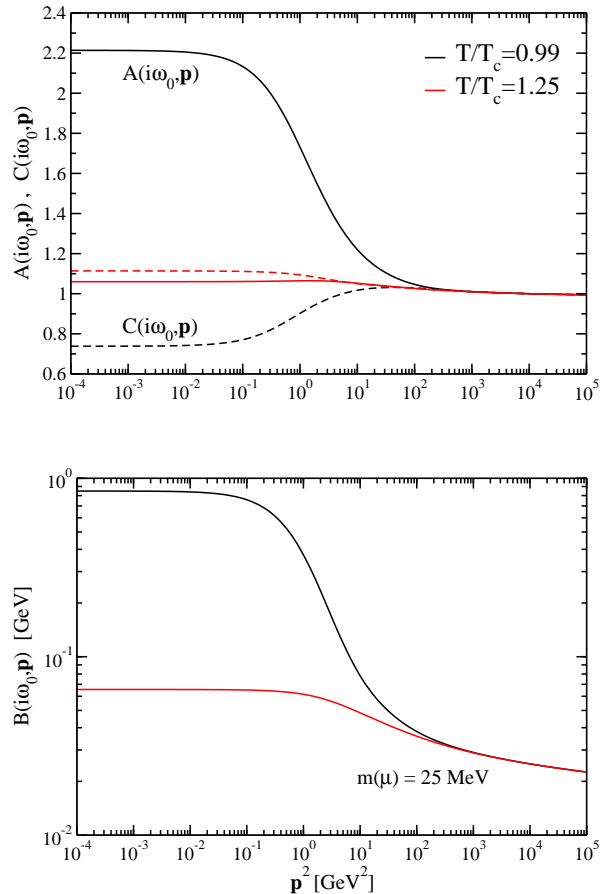


FIG. 2: Momentum dependence of the dressing functions  $A$ ,  $C$ ,  $B$  below and above the critical temperature. Results are shown for the lowest Matsubara frequency and finite bare quark mass  $m(\boldsymbol{\mu}) = 25 \text{ MeV}$ .

of constant dressing functions this is perfectly consistent with our expectations: As can be seen from Eq. (3), we would interpret  $\sqrt{A/C} = v \leq 1$  as the velocity of the quasiparticles,  $\sqrt{v^2 \mathbf{p}^2 + B^2/C^2}$  as their dispersion relation and  $1/C \leq 1$  as the wave-function renormalization of the  $\gamma_4$ -component<sup>1</sup>. In contrast to the HTL approximation there is, however, a momentum range (8  $\text{GeV}^2$  to 200  $\text{GeV}^2$  in Fig. 2) where  $A(i\omega_0, \mathbf{p}) > C(i\omega_0, \mathbf{p})$  for all here considered temperatures above  $T_c$  and all masses. To what extent this behavior is generic or truncation-affected needs to be investigated in future studies.

Below  $T_c$ , on the contrary, the results become less intuitive. Due to the stronger interaction and lower temperature, the chiral symmetry breaking dressing function  $B$  is significantly larger in the infrared with its size related to the scale of dynamical symmetry breaking. For the dressing functions  $A(i\omega_0, \mathbf{p})$  and  $C(i\omega_0, \mathbf{p})$  we find,

<sup>1</sup> Note that only the  $\gamma_4$ -component of the quark propagator obeys a sum rule [23].

however,  $A(i\omega_0, \mathbf{p}) > C(i\omega_0, \mathbf{p})$ . This does not allow for a simple quasiparticle interpretation as outlined above. Also the contribution from the self-energy is of the same order as the free propagator, in particular the dressing function  $A(i\omega_0, \mathbf{p})$  is strongly enhanced in the infrared. This also hints towards more complicated dynamics than a gas of quasiparticles, which is of course expected in the confined phase of QCD.

From these results we therefore conclude that a simple interpretation in terms of the excitation spectrum seems not appropriate below  $T_c$ . Even for the analysis above  $T_c$ , as we discuss in the following, the quasiparticles can receive a thermal mass in the chirally restored phase. This is already known from the HTL expansion, where the quasiparticles in the high temperature and small coupling regime have a mass of order  $gT$ .

#### IV. QUARK SPECTRAL FUNCTIONS AND REPRESENTATION

Causality and resulting analyticity imply that a correlator can be represented through a spectral function. For the quark propagator this representation is given by

$$S(i\omega_n, \mathbf{p}) = \int_{-\infty}^{\infty} \frac{d\omega'}{2\pi} \frac{\rho(\omega', \mathbf{p})}{i\omega_n - \omega'}, \quad (8)$$

where the Dirac structure of the spectral function is parameterized as

$$\rho(\omega, \mathbf{p}) = 2\pi(\rho_4(\omega, |\mathbf{p}|)\gamma_4 + \rho_v(\omega, |\mathbf{p}|)(i\boldsymbol{\gamma} \cdot \mathbf{p})/|\mathbf{p}| - \rho_s(\omega, |\mathbf{p}|)). \quad (9)$$

Our conventions are chosen such that the scalar dressing functions themselves agree with those introduced in Ref. [25] using Minkowski space conventions<sup>2</sup>. Assuming a positive definite Fock space<sup>3</sup>, the dressing functions furthermore obey

$$\rho_4(\omega, |\mathbf{p}|) \geq \sqrt{\rho_v(\omega, |\mathbf{p}|)^2 + \rho_s(\omega, |\mathbf{p}|)^2} \geq 0 \quad (10)$$

and the sum rules

$$1 = Z_2 \int_{-\infty}^{\infty} d\omega \rho_4(\omega, |\mathbf{p}|), \quad (11)$$

$$0 = \int_{-\infty}^{\infty} d\omega \rho_v(\omega, |\mathbf{p}|), \quad (12)$$

$$0 = \int_{-\infty}^{\infty} d\omega \rho_s(\omega, |\mathbf{p}|), \quad (13)$$

where here  $Z_2$  is the wave function renormalization constant and not the plasmino residue which will be introduced later.

In the following we limit ourselves to vanishing momenta  $|\mathbf{p}|$  and the chirally restored phase, respectively. For this purpose it is instructive to introduce the projectors

$$P_{\pm}(\mathbf{p}) = \frac{1}{2}(1 \mp i\gamma_4 \boldsymbol{\gamma} \cdot \mathbf{p}/|\mathbf{p}|), \\ L_{\pm} = \frac{1}{2}(1 \mp \gamma_4), \quad (14)$$

where the signs are again chosen in order to agree with common Minkowski space conventions.  $P_{\pm}(\mathbf{p})$  can be interpreted as energy projectors for massless modes.

For vanishing momentum it is then convenient to write

$$\rho(\omega, \mathbf{0}) = \rho_+^M(\omega)L_+\gamma_4 + \rho_-^M(\omega)L_-\gamma_4, \quad (15)$$

$$S(i\omega_n, \mathbf{0}) = S_+^M(i\omega_n)L_+\gamma_4 + S_-^M(i\omega_n)L_-\gamma_4, \quad (16)$$

i.e.  $\rho_{\pm}^M(\omega) = 2\pi(\rho_4(\omega, \mathbf{0}) \pm \rho_s(\omega, \mathbf{0}))$  and  $\rho_v(\omega, \mathbf{0}) = 0$ . From Eqs. (10) and (13) we infer that the functions  $\rho_{\pm}^M(\omega)$  are positive semi-definite and normalized to  $2\pi Z_2$ . Furthermore the spectral representation yields the scalar relation

$$S_{\pm}^M(i\omega_n) = \int_{-\infty}^{\infty} \frac{d\omega'}{2\pi} \frac{\rho_{\pm}^M(\omega')}{i\omega_n - \omega'}. \quad (17)$$

On the other hand for a chirally symmetric phase with  $B(i\omega, |\mathbf{p}|) = 0$  and  $\rho_s(\omega, |\mathbf{p}|) = 0$ , we introduce

$$\rho(\omega, \mathbf{p}) = \sum_{e=\pm} \rho_e^P(\omega, |\mathbf{p}|) P_e(\mathbf{p}) \gamma_4, \quad (18)$$

$$S(i\omega_n, \mathbf{p}) = \sum_{e=\pm} S_e^P(i\omega_n, |\mathbf{p}|) P_e(\mathbf{p}) \gamma_4, \quad (19)$$

i.e.  $\rho_{\pm}^P(\omega, |\mathbf{p}|) = 2\pi(\rho_4(\omega, |\mathbf{p}|) \pm \rho_v(\omega, |\mathbf{p}|))$ . As before we see that  $\rho_{\pm}^P(\omega, |\mathbf{p}|)$  is positive semi-definite and normalized to  $2\pi Z_2$ . The spectral representation for the dressing functions again take the form

$$S_{\pm}^P(i\omega_n, |\mathbf{p}|) = \int_{-\infty}^{\infty} \frac{d\omega'}{2\pi} \frac{\rho_{\pm}^P(\omega', |\mathbf{p}|)}{i\omega_n - \omega'}. \quad (20)$$

In the following we aim to invert the linear relation between Matsubara propagators  $S_{\pm}^M(i\omega_n)$ ,  $S_{\pm}^P(i\omega_n, \mathbf{p})$  determined by solving the truncated DSE and the respective spectral functions  $\rho_{\pm}^M(\omega)$  and  $\rho_{\pm}^P(\omega, |\mathbf{p}|)$ . Strictly speaking, for a finite set of Matsubara frequencies, this problem is however ill-posed.

#### V. QUARK SPECTRAL FUNCTIONS AT ZERO MOMENTUM

In this section we focus our attention to the quark propagator at zero momentum. We analyze the correlator at temperatures below and above the critical temperature and for various bare quark masses. Since the

<sup>2</sup>  $\gamma_M^\mu$  in common Minkowski space conventions are related to those used in this work via  $\gamma_M^0 = -\gamma_4$  and  $\gamma_j = -i\gamma_M^j$ .

<sup>3</sup> For completeness we note that this is not guaranteed for a gauge-fixed Yang-Mills theory.



general problem of extracting the spectral function from the spectral representation is ill-posed, we will limit ourselves to parameterized ansätze and determine the best fitting function in the given subspace. Above the critical temperature we study the quark mass dependence of the so obtained insight on quasiparticle excitations. This strategy was explored in Refs.[24, 25] in the framework of lattice QCD.

We will mainly consider the following two-pole ansatz for the spectral function

$$\rho_{\pm}^M(\omega) = 2\pi[Z_1\delta(\omega \mp E_1) + Z_2\delta(\omega \pm E_2)], \quad (21)$$

with fitting parameters  $Z_1$ ,  $Z_2$  and  $E_1$ ,  $E_2$ . This will be related to our quark propagator via Eq. (17), for which we identify

$$S_{\pm}^{\text{DSE}, M}(i\omega_n) = -\frac{i\omega_n C(i\omega_n, 0) \pm B(i\omega_n, 0)}{\omega_n^2 C^2(i\omega_n, 0) + B^2(i\omega_n, 0)}. \quad (22)$$

Our choice is suggested by HTL results at high temperatures and small coupling. In contrast to a non-interacting fermion, whose spectral function consists of a single  $\delta$ -function, it is known from HTL that an additional collective excitation develops: the plasmino. The fitting parameters  $E_{1,2}$  denote the quasiparticle energies and  $Z_{1,2}$  the corresponding residues. Certainly the full spectral function will be more complicated. The working assumption here is, that if quasiparticle excitations with small decay widths exist, then their peaks will be the dominant contribution of the spectral function and therefore such a simple ansatz may reveal characteristics of the quasiparticles and their dispersion relations. However, we emphasize again that in HTL calculations the thermal masses  $E_{1/2}$  are of order  $gT$ , whereas the width of the corresponding peaks in the spectral functions are of order  $g^2T$ . In a strong coupling regime this becomes of the same order, if not larger.

Likewise as done in Ref. [25] we also investigated other ansätze for the spectral function. We considered a single pole ansatz

$$\rho_{\pm}^M(\omega) = 2\pi Z_1\delta(\omega \mp E_1), \quad (23)$$

and ansätze allowing for one- and two-particle excitations with Gaussian widths

$$\rho_{\pm}^M(\omega) = 2\sqrt{\pi} \frac{Z_1}{\Gamma_1} \exp \frac{-(\omega \mp E_1)^2}{\Gamma_1^2}, \quad (24)$$

$$\rho_{\pm}^M(\omega) = 2\sqrt{\pi} \left[ \frac{Z_1}{\Gamma_1} \exp \frac{-(\omega \mp E_1)^2}{\Gamma_1^2} + \frac{Z_2}{\Gamma_2} \exp \frac{-(\omega \pm E_2)^2}{\Gamma_2^2} \right]. \quad (25)$$

Here  $\Gamma_1$  and  $\Gamma_2$  are additional fitting parameters.

In order to evaluate the quality of the fit we minimize

$$\ell_{\pm}^2 = \sum_n^{N_{\omega}} \left| S_{\pm}^{\text{DSE}, M}(i\omega_n) - S_{\pm}^M(i\omega_n) \right|^2, \quad (26)$$

i.e. we implicitly assume uncorrelated data with equal total errors. For comparing the different fit forms we evaluate  $\ell_{\pm}^2$  with  $N_{\omega} = 39$ . In principle, one may also define  $\ell_{\pm}^2/\text{dof}$  where dof denotes  $N_{\omega}$  minus the number of fit parameters however this does not affect our results.

A remark on the numerical results seems appropriate here. Within a given truncation scheme the error in Dyson-Schwinger calculations is essentially determined by the error of the numerical integration. It can be estimated by varying the numerical parameters of the integration and can be made significantly smaller than in lattice calculations. At least for large temperatures where the Matsubara frequencies are largely separated, the assumption of uncorrelated errors seems reasonable. In principle, the self-energy is calculated in DSE calculations and the total error appears for the inverse propagator, which grows linearly in frequencies  $\omega_n$ . By using Eq. (26) we therefore enhance the importance of small  $\omega_n$ . We expect the relevant information for spectral functions to be encoded here as the propagator approaches the perturbative result at large frequencies very fast.

For the data analyzed we find  $\ell_{\pm}^2$  more than one order of magnitude smaller for fits based on Eq. (21) than for the single pole Ansatz Eq. (23). This is in accordance with the findings in Ref. [25]. Comparing  $\ell_{\pm}^2$  obtained from the single peak ansatz Eq. (24) with its value obtained for ansatz (21) we find similar results for light quarks ( $m/T \lesssim 0.2$ ) but roughly one order of magnitude difference in favor of (21) for heavy quarks ( $m/T \gtrsim 0.2$ ).

Examining ansatz (25) we find parameters with improved  $\ell_{\pm}^2$  compared to the two pole ansatz. However depending on the initial parameter values different local minima may be found. Typical solutions correspond to a normal mode with a width which tends to zero and a plasmino mode with broad width. Furthermore we find that the possible excitations do not acquire a thermal mass in the chiral limit. In Ref. [25] it was found that ansatz (25) may improve  $\chi^2/\text{dof}$  for uncorrelated fits but reduces to two delta functions for correlated fits. By way of comparison and taking into account the results of [25] for correlated data we focus the discussion to the two-pole ansatz in the following.

### A. Results above and below the critical temperature

Before analyzing the quark mass dependence of the fit parameters we investigate the propagator below and above the critical temperature. Here,  $T_c$  is given by the deconfinement transition as extracted from the lattice simulations of our input gluon propagator and from the dressed Polyakov loop extracted from the quark propagator, see [32] for details. The chiral transition temperature coincides with  $T_c$  within a few MeV, depending slightly on the bare quark mass.

In Fig. 3 we show the Schwinger function defined by

the Fourier transform of  $S_+^M(i\omega_n)$ :

$$S_+^M(\tau) = -T \sum_n e^{-i\omega_n \tau} S_+^M(i\omega_n). \quad (27)$$

The numerical data are denoted by data points. Above  $T_c$  the solid lines are obtained by using the spectral function obtained from fitting with ansatz (21). Note that the points close to  $\tau T = 0$  and  $\tau T = 1$  are subject to boundary effects due to the finite number of Matsubara modes used when Fourier transforming.

At zero temperature the Schwinger function has been used to search for positivity violations in the quark propagator. From the Osterwalder-Schrader axioms of Euclidean quantum field theory one knows that the Schwinger function needs to be strictly positive for physical particles. Conversely, positivity violations in the Schwinger function are a sufficient criterion for the absence of the corresponding particle from the physical spectrum of a theory. Using the spectral representation (17) in Eq. (27) it is also easy to see, that a positive spectral function always gives a positive Schwinger function. For the quark propagator at zero temperature these properties have been investigated in a number of works, see [40] and Refs. therein. At finite temperature it has been suggested from calculations in a simple model, that positivity violations only occur below the critical temperature, whereas positivity is restored above  $T_c$  [41]. Although this is not exactly what we see in our more elaborate calculation, there are clear signals for a qualitative change in the Schwinger function at  $T_c$ . This is in line with quenched lattice QCD results that directly determine  $S_+^M(\tau)$  [25].

Above the critical temperature  $S_+^M(\tau)$  is positive and found to be convex on a log-scale. Furthermore chiral symmetry restoration through  $B(i\omega_n, 0) = 0$  translates into  $S_+^M(i\omega_n) = -S_+^M(-i\omega_n)$  and  $S_+^M(\tau) = S_+^M(1/T - \tau)$ . We see this symmetry emerge when decreasing the current quark mass  $m(\mu)$ . Related to dynamical symmetry breaking this symmetry is absent below  $T_c$ , even in the chiral limit. More striking, however, is the concave shape around  $\tau T \approx 0.5$  on a log-scale. This cannot be reproduced by any ansatz including real poles only. This finding again agrees with quenched lattice calculations in Ref. [25].

In addition we find positivity violations at  $T = 0.99 T_c$  for a range in current quark masses, albeit this effect is not seen in the chiral limit and also for the smaller temperature. Nevertheless, the concaveness of the Schwinger function below  $T_c$  is generic in the sense that it is independent of variations in  $d_1$ . It can also not be attributed to the dynamical generation of quark masses: we find concave curvature below the deconfinement transition temperature  $T_c$  also in the chiral limit and for values of  $d_1$  that do not allow for spontaneous dynamical mass generation. It is therefore apparent, that the curvature of the Schwinger function is related to quark confinement [41] and may serve as another source for extracting the

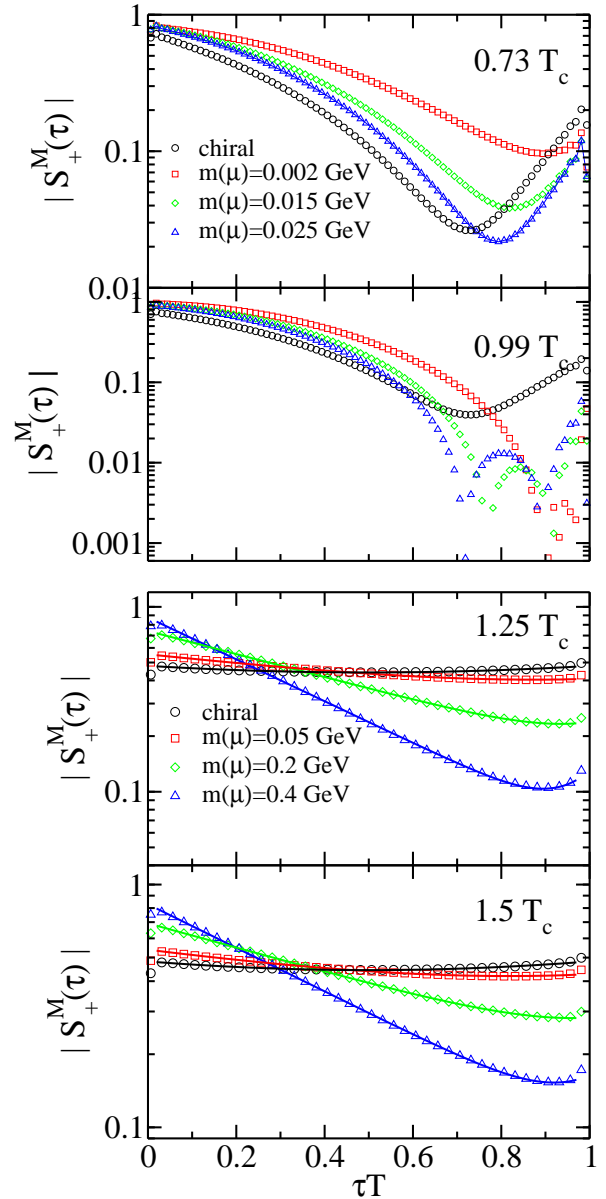


FIG. 3: Schwinger function  $S_+^M(\tau)$  for different temperatures and current quark masses. For  $T = 0.99 T_c$  and  $m(\mu) = 0.2, 0.4 \text{ GeV}$  the Schwinger function changes sign in an interval around  $\tau T \approx 0.8$ .

deconfinement transition temperature  $T_c$  from the quark propagator besides the dressed Polyakov loop [29, 31, 42].

### B. Quark mass dependence of fit parameters

In the upper part of Fig. 4 the dependence of the poles  $E_1, E_2$  on the current quark mass for three different temperatures is shown. The lower part shows the relative strength of the plasmino pole, defined as the  $E_2$  branch in the upper plot, which is given by the ratio  $Z_2/(Z_1 + Z_2)$ . The disappearance of the scalar part of the

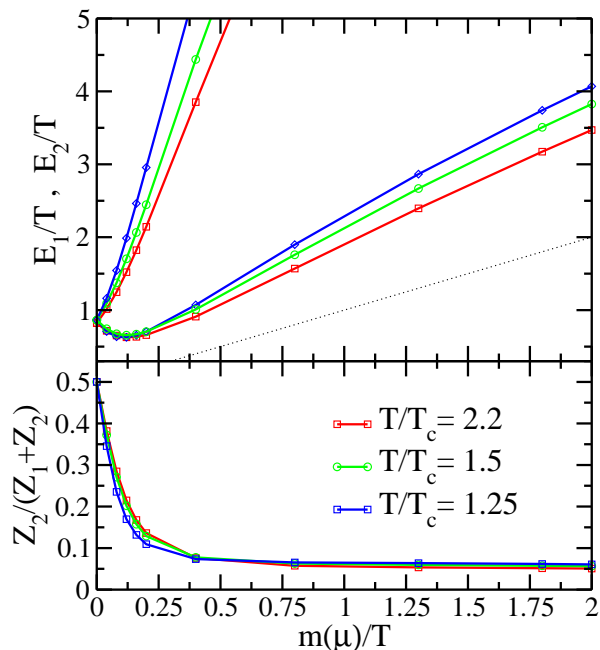


FIG. 4: Dependence of fit parameters in two-pole ansatz at vanishing momentum on current quark mass  $m(\mu)$  for three temperatures. For the two branches in the upper plot we define  $E_2 \geq E_1$ .

propagator in the chiral limit, i.e.  $B(i\omega_n, 0) = 0$ , manifests itself in the spectral function being an even function,  $\rho(-\omega, \mathbf{0}) = \rho(\omega, \mathbf{0})$ , and therefore  $E_1 = E_2$ ,  $Z_1 = Z_2$ . We use this as the definition of the thermal mass  $m_T \equiv E_1$  and, as outlined in the context of Tab. I, use this value to determine the vertex parameter  $d_1$ . It is worth noting that the qualitative behavior in Fig. 4 does not change when increasing  $d_1$  by one order of magnitude.

From the mass dependence of  $Z_2/(Z_1 + Z_2)$  in Fig. 4 it is discernible that the plasmino contribution decreases with increasing quark mass. This is in accordance with the expectation that for heavy quarks the spectral function reduces to one of free quarks. Only small deviations from sum rule (11) are found with a mismatch of less than 4%. Furthermore we find the minimum of  $E_1$  at non-vanishing quark mass whereas the plasmino pole increases monotonically with quark mass. The slope of  $E_1$  and  $E_2$  for fixed  $m(\mu)/T$  is temperature dependent and decreases with increasing temperature. Compared to the lattice data in Ref. [25] we find qualitative and quantitative similar results. The minima in  $E_1$  approximately coincide with the lattice results whereas the slopes in  $Z_2/(Z_1 + Z_2)$  and  $E_{1,2}$  are slightly different. However this may be traced back to different definitions of the bare quark mass.

## VI. MOMENTUM DEPENDENCE OF THE SPECTRAL FUNCTION IN THE CHIRAL LIMIT

In this section we investigate the quark propagator in the chiral limit for varying momenta. For a chirally symmetric quark propagator it is convenient to use the decomposition on energy projectors as shown in Eqs. (18) and (19). In terms of the quark dressing functions we then have

$$S_{\pm}^P(i\omega_n, |\mathbf{p}|) = -\frac{i\omega_n C(i\omega_n, |\mathbf{p}|) \pm |\mathbf{p}| A(i\omega_n, |\mathbf{p}|)}{\omega_n^2 C^2(i\omega_n, |\mathbf{p}|) + |\mathbf{p}|^2 A^2(i\omega_n, |\mathbf{p}|)}. \quad (28)$$

Along the same line as in the previous section we use the two-pole ansatz

$$\rho_{\pm}^P(\omega, |\mathbf{p}|) = 2\pi [Z_1 \delta(\omega \mp E_1) + Z_2 \delta(\omega \pm E_2)] \quad (29)$$

and fit the parameters  $Z_1$ ,  $Z_2$  and  $E_1$ ,  $E_2$  to the data. These are then momentum dependent and we obtain the dispersion relation of quasiparticle and plasmino together with their spectral strength. For all momenta shown here  $\ell_{\pm}^2$  is of the same order of magnitude than the results for zero momentum.

In Fig. 5 we show the results for the momentum dependence of the parameters  $E_1$ ,  $E_2$  and  $Z_2/(Z_1 + Z_2)$  for temperatures  $T/T_c = 1.25, 1.5$  and  $2.2$ . For increasing momenta the ratio  $Z_2/(Z_1 + Z_2)$  decreases and tends to go to zero for high momenta. Likewise  $E_1$  is approaching the light cone. Therefore the spectral function at high momenta reduces to the one of a single free particle. In the plasmino branch a minimum at non-vanishing momentum is clearly recognizable. This feature is known from perturbation theory and may be anticipated from the results in Ref. [25]. It is conspicuous and not obtained in one loop perturbation theory that the plasmino branch goes over into the space-like region. However it is known that due to Landau damping the spectral function at high temperatures contains a contribution in the space-like region which is not included in our fit ansatz Eq. (29). It might be that the plasmino pole by shifting into the space-like region mimics this missing contribution. This possibility is also considered in the following. An analytic continuation of the DSE to include smaller Euclidean energies might help to distinguish these different scenarios. Also note that with increasing momenta, the value of  $E_2$  becomes less constrained by the fitting procedure, since the spectral strength  $Z_2$  and therefore the contribution of the plasmino branch to the data decreases.

In Fig. 6 we focus on the region near zero momentum. In addition to the fitted values shown as straight lines, we also present the behavior for the HTL result [39] given by

$$E_1 \simeq m_T + \frac{|\mathbf{p}|}{3}, \quad E_2 \simeq m_T - \frac{|\mathbf{p}|}{3}, \quad (30)$$

$$\frac{Z_2}{Z_1 + Z_2} \simeq \frac{1}{2} - \frac{|\mathbf{p}|}{3m_T} \quad (31)$$



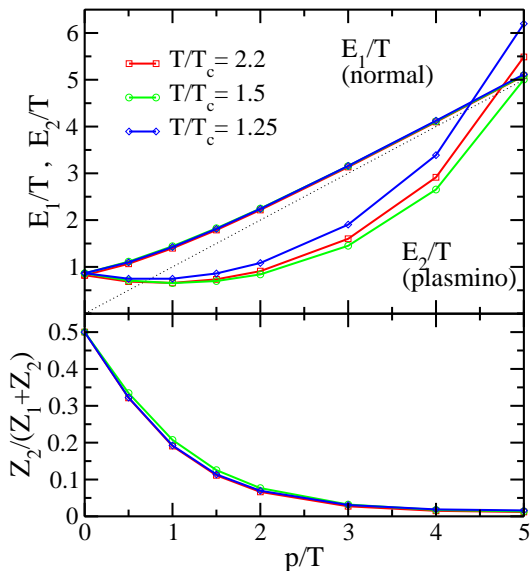


FIG. 5: Momentum dependence of the fit parameters for the two pole ansatz (29) at three different temperatures.

for  $|\mathbf{p}| \ll m_T$ . We observe that our results agree well with the HTL result for sufficiently small momentum, with the better agreement for the plasmino branch  $E_2$ , and then depart from it. Since the expansion is supposed to apply for small  $|\mathbf{p}|/T$ , this is expected. Comparing the two temperatures it is recognizable that the results at higher temperature agree better with the HTL result, although we are certainly not in a regime where we expect the HTL approximation to work.

Since the result for the plasmino branch of the two-pole ansatz indicate a possible space-like continuum contribution we extend the two-pole ansatz (29) by the HTL continuum contribution. The fitting function then matches exactly the spectral function in HTL approximation

$$\begin{aligned} \rho_{\pm}^P(\omega, |\mathbf{p}|) &= 2\pi [Z_1 \delta(\omega \mp E_1) + Z_2 \delta(\omega \pm E_2)] \\ &+ \frac{\pi}{|\mathbf{p}|} m_T^2 (1 \mp x) \Theta(1 - x^2) \\ &\times \left[ \left( |\mathbf{p}| (1 \mp x) \pm \frac{m_T^2}{2|\mathbf{p}|} \left[ (1 \mp x) \right. \right. \right. \\ &\left. \left. \left. \times \ln \left| \frac{x+1}{x-1} \right| \pm 2 \right] \right)^2 + \frac{\pi^2 m_T^4}{4|\mathbf{p}|^2} (1 \mp x)^2 \right]^{-1} \end{aligned} \quad (32)$$

where  $x = \omega/|\mathbf{p}|$ . The thermal masses are taken from Tab. I and  $E_{1,2}$  and  $Z_{1,2}$  are the fit parameters. The results are shown in Fig. 7. We find  $\ell_+^2$  to be marginally smaller compared to the two-pole ansatz and we conclude from the results presented in Fig. 5, that the plasmino branch going over into the space-like region might well be an artifact of a missing space-like spectral weight in ansatz (21). The upper plot of Fig. 7 shows that the plasmino tends to the light cone for momenta  $p/T \simeq 0.8$  instead of crossing it. Also the minimum of the plasmino branch has shifted to lower momenta. At high momenta

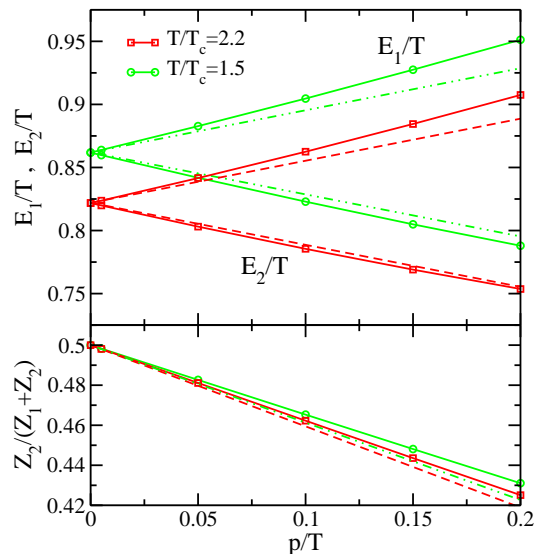


FIG. 6: Close up of Fig. 5 in momentum range  $p/T \in [0, 0.2]$ . For comparison we give the small momentum behavior of the HTL approximation in Eqs.(30) and (31) as dashed lines.

the plasmino seems to deviate from the light cone again. However we note again that due to the small spectral strength  $Z_2$  at these momenta the value of  $E_2$  is only poorly constrained. On the other hand the momentum dependence of  $E_1$  is practically unaltered.

The lower plot of Fig. 7 shows the relative strength of the plasmino  $Z_2/Z_{\text{tot}}$  where

$$Z_{\text{tot}} = Z_1 + Z_2 + \int_{-|\mathbf{p}|}^{+|\mathbf{p}|} d\omega \rho_{\pm}^P(\omega, |\mathbf{p}|). \quad (33)$$

Compared to the two-pole ansatz the plasmino spectral weight decreases considerably more rapid with increasing momentum. We also find that  $Z_{\text{tot}}$  agrees within 3% with the expected value obtained from sum rule (11). Since the spacelike part is subleading for small momenta the small momentum behavior of  $E_{1,2}$  and  $Z_2/(Z_1 + Z_2)$  is practically unaltered by the continuum contribution.

## VII. QUARK SPECTRAL FUNCTIONS VIA MEM

In order to shed more light on the possible shape of the spectral functions and also on the truncation for gluon propagator and quark-gluon vertex<sup>4</sup>, we employ MEM. For simplicity our discussion will be based on historical

<sup>4</sup> Note that their parameterization used here is only constrained in Euclidean space, but their analytic continuation is in principle relevant for the shape of the quark spectral function.

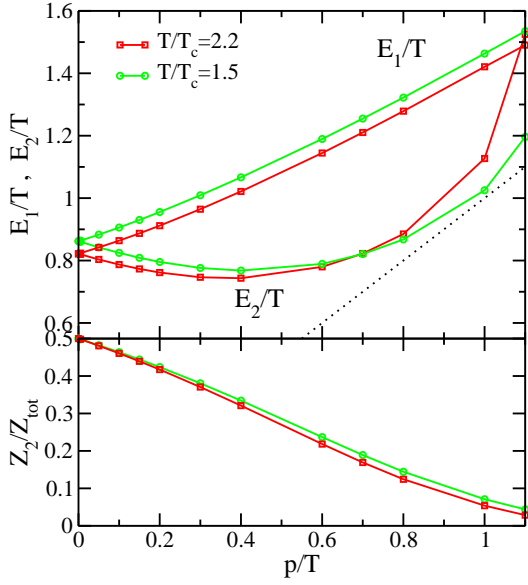


FIG. 7: Momentum dependence of the fit parameters for the extended ansatz (32) for two different temperatures.

MEM (see e.g. Refs. [19, 20]), where we maximize the functional

$$Q[\rho] = \alpha S[\rho] - \frac{1}{2} \chi^2[\rho] \quad (34)$$

in the spectral function  $\rho$ . Its constituents are the entropy  $S[\rho]$  and the  $\chi^2[\rho]$ -distribution. In the case of a scalar channel as in Eq. (17) and Eq. (20) it is common to use the Shannon-Jaynes entropy

$$S[\rho_{\pm}] = \int d\omega \left( \rho_{\pm}(\omega) - m(\omega) - \rho_{\pm}(\omega) \log \left( \frac{\rho_{\pm}(\omega)}{m(\omega)} \right) \right) \quad (35)$$

for the entropy functional with prior estimate  $m(\omega)$ . Features of this choice are that there is only one minima in  $Q[\rho]$  for each choice of  $m(\omega)$  and that  $\rho(\omega)$  has the same sign as  $m(\omega)$ . For the  $\chi^2[\rho]$ -distribution between the propagator given through  $\rho(\omega)$  and the data from DSE calculations we will assume

$$\chi^2[\rho_{\pm}] = \frac{1}{\sigma^2} \ell_{\pm}^2. \quad (36)$$

As discussed before this corresponds to assuming uncorrelated data with equal errors and we will need to specify the variance  $\sigma^2$ . For the prior estimate, which essentially determines the support of the spectral function and its semi-positivity, we assume

$$m(\omega) = m_0 \theta(\Lambda^2 - \omega^2). \quad (37)$$

The magnitude  $m_0$  and the cutoff  $\Lambda$  will be varied in the following to analyze their influence on the shape of the extracted spectral function. The method as presented here follows the philosophy of regularization [19]: Since

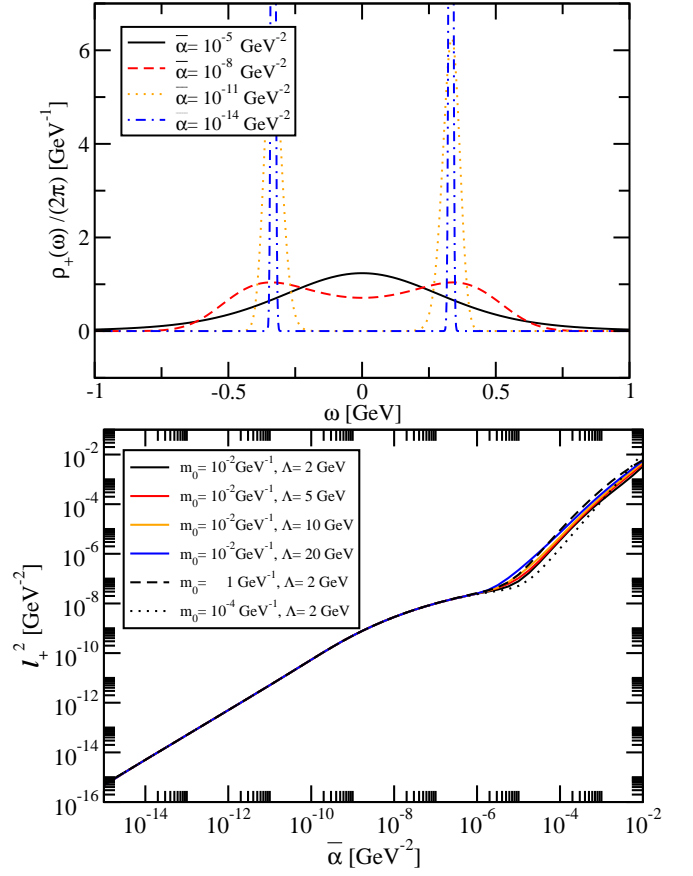


FIG. 8: Upper panel: Spectral function extracted from 'mock' data at various values of  $\bar{\alpha}$  for  $m_0 = 10^{-2} \text{GeV}^{-1}$  and  $\Lambda = 2 \text{GeV}$ . Lower panel:  $\ell_+^2$  as function of  $\bar{\alpha}$  for various  $m_0$  and  $\Lambda$ . For both plots we have  $T = 1.5T_c$ ,  $M = 0.8 \times 1.5T_c$  and  $N_\omega = 20$ .

the inversion of the spectral representation is an ill-posed problem, we want to impose the positivity condition on the spectral function in a way that leads to a well-defined problem.

In historical MEM the Lagrange multiplier  $\alpha$  is then chosen such that  $\chi^2[\rho_{\pm}] = N_\omega$ . Within our setup we observe, however, that the extracted spectral functions  $\rho_{\pm}(\omega)$  actually only depends on the combination  $\bar{\alpha} = \alpha\sigma^2$  and that in this case  $\sigma^2 = \ell_{\pm}^2/N_\omega$ . We will exploit this feature by varying  $\bar{\alpha}$  in the following, in particular because we do not want to give an estimate for  $\sigma^2$  at this point.

In order to get an intuition for the way MEM works, we consider  $\mathbf{p} = 0$  and produce 'mock data' by determining  $S_+(\omega_n)$  for the spectral function

$$\rho_+(\omega) = 2\pi \left( \frac{1}{2} \delta(M - \omega) + \frac{1}{2} \delta(M + \omega) \right) \quad (38)$$

analytically. This corresponds to the two-pole ansatz (21) and also with the HTL result at  $\mathbf{p} = 0$ .

Our results are summarized in Fig. 8. By the example

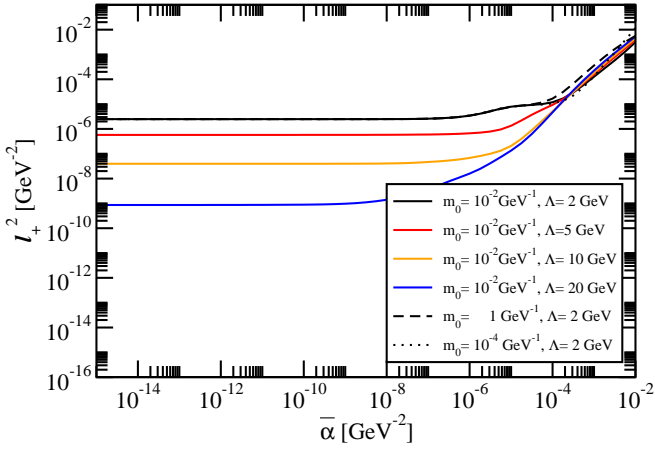


FIG. 9:  $\ell_+^2$  between numerical DSE results and  $S_+(\omega_n)$  for MEM extracted spectral function as a function of  $\bar{\alpha}$  for various  $m_0$  and  $\Lambda$  as well as  $T = 1.5 T_c$  and  $N_\omega = 20$ .

of  $m_0 = 10^{-2}\text{GeV}^{-1}$  and  $\Lambda = 2\text{GeV}$ , we observe that the correct spectral function is reproduced when making  $\bar{\alpha}$  sufficiently small. This is very generic, in particular we checked that the extracted spectral function for a given  $\bar{\alpha} \in [10^{-15}\text{GeV}^{-2}, 10^{-5}\text{GeV}^{-2}]$  is indistinguishable on the plot when varying  $m_0 \in [1\text{GeV}^{-1}, 10^{-4}\text{GeV}^{-1}]$  and  $\Lambda \in [2\text{GeV}, 20\text{GeV}]$ . For the corresponding  $\ell_+^2$ , which should be equal to  $N_\omega\sigma^2$  by choosing an appropriate  $\alpha$ , we find on the one hand side, that the dependence on the prior estimate is most extreme at larger  $\bar{\alpha}$ , albeit in general the sensitivity can be considered as mild. More importantly, we find that  $\ell_+^2$  for different prior estimates converges quickly upon decreasing  $\bar{\alpha}$  and that it converges towards zero. This can be qualitatively understood from the fact that we know that there is a positive definite spectral function which reproduces the data and that there is a competition between  $\alpha S[\rho_+]$  and  $\frac{1}{2}\chi^2[\rho_+]$  when maximizing the functional  $Q[\rho_+]$ . This leads to  $\alpha S[\rho_+] \sim \frac{1}{2}\chi^2[\rho_+]$  and  $S[\rho_+] \rightarrow \text{const} > 0$ . Consequently,  $\ell_+^2$  should go to zero when taking  $\bar{\alpha} \rightarrow 0$ .

Before discussing errors on our computed DSE 'data', we want to present the results when applying MEM to our results in a similar fashion as discussed above. For this purpose we present  $\ell_+^2$  as a function of  $\bar{\alpha}$  at  $\mathbf{p} = 0$  for various prior estimates in Fig. 9 and illustrate some extracted spectral functions for  $m_0 = 10^{-2}\text{GeV}^{-1}$  as well as  $\Lambda = 10\text{GeV}$  and  $\Lambda = 20\text{GeV}$  in Fig. 10.

The two-pole fit ansatz (21) for this specific case yields  $\ell_+^2 \approx 10^{-5}\text{GeV}^{-2}$ . As anticipated we obtain better fitting spectral functions for small enough  $\bar{\alpha}$ , here  $\bar{\alpha} \lesssim 10^{-5}\text{GeV}^{-2}$  for the considered prior estimates  $m_0 \in [1\text{GeV}^{-1}, 10^{-4}\text{GeV}^{-1}]$  and  $\Lambda \in [2\text{GeV}, 20\text{GeV}]$ . As before we also find that the dependence on  $m_0$  is very weak and we can therefore focus on the spectral function's support given through  $\Lambda$  only. It is, however, striking that the  $\ell_+^2$  has a strong dependence on  $\Lambda$ . Of course we should be able to obtain better fitting spectral function

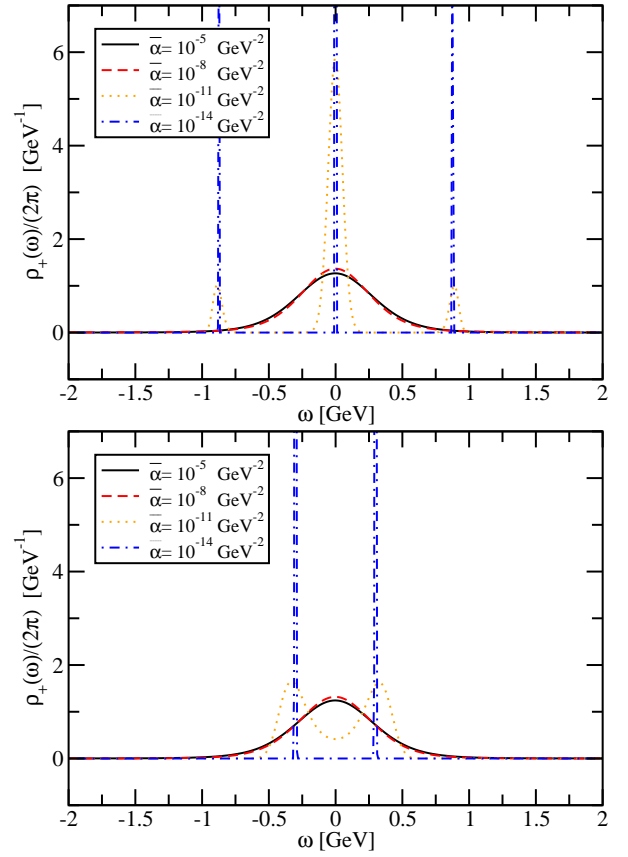


FIG. 10: Upper panel: Spectral functions extracted from numerical DSE results at various values of  $\bar{\alpha}$  for  $m_0 = 10^{-2}\text{GeV}^{-1}$ ,  $\Lambda = 10\text{GeV}$  and  $N_\omega = 20$ . Lower panel: Same as upper plot but for  $\Lambda = 20\text{GeV}$ .

when increasing the support, the results suggest however that a few percent of the spectral strength come from energies  $|\omega| > 2\text{GeV}$  near  $\Lambda$ . This is unexpected. As shown in Fig. 10 this does not affect the shape of the extracted spectral function in the domain  $\omega \in [-2\text{GeV}, 2\text{GeV}]$  for  $\bar{\alpha} \approx 10^{-8}\text{GeV}^{-2}$  noticeably. In case of the mock data we could already observe a two-peak structure at this point.

When decreasing  $\bar{\alpha}$  beyond  $10^{-8}\text{GeV}^{-2}$ , we find a strong dependence on  $\Lambda$  and even more puzzling a fast saturation of  $\ell_+^2$ . The fact that the spectral functions tend towards a sum of peaked functions should be considered a generic feature of method and not be over-interpreted. The agreement at  $\Lambda = 20\text{GeV}$  with the two-pole ansatz is probably a coincidence, in particular since the true spectral function is expected to have a finite width.

The reason for our conservatism is the value of  $\ell_+^2$  that can be obtained within MEM. Even for an allowed support of  $[-20\text{GeV}, 20\text{GeV}]$ , we cannot obtain  $\ell_+^2 \leq 8 \cdot 10^{-10}\text{GeV}^{-2}$ . On the other hand a variation of numerical parameters suggests that the numerical error on our 'data' is in fact below this value. Therefore, strictly speaking, historical MEM requiring  $\chi^2 = N_\omega$  can-

not be applied.

A plausible explanation for this finding would be a spectral function that, at least for the applied truncation scheme, is not positive semi-definite. To elaborate this a bit further, it is known e.g. from the calculation in Ref. [18], that the determination of the spectral functions via the quark's DSE requires knowledge of gluon-propagator and quark-gluon vertex in the time-like domain and in particular of the gluon's spectral function. For the parameterization of the gluon used in this work, it can be checked that its spectral function is not positive semi-definite.

We therefore consider the analysis via MEM on the one hand side as an advise for caution when looking at the fits discussed in the earlier sections. On the other hand it motivates future work for the direct determination of the spectral function and a better analysis of the truncation scheme.

### VIII. CONCLUSIONS AND OUTLOOK

In the present work we have analyzed the quark propagator at finite temperatures obtained within a recently employed truncation of the quark's Dyson-Schwinger equation. The investigation was in part motivated by lattice QCD calculations of the quark propagator in Landau gauge using the quenched approximation, which - in addition - also attempted to extract the spectral function of the propagator from the obtained data.

For the Matsubara propagator, i.e. in Euclidean space, we found qualitative agreement with the lattice QCD results below and above the deconfinement phase transition. General analytic properties of the quark propagator are different below and above the deconfinement phase transition temperature and as our results indicate, determined by the non-perturbative behavior of the gluon propagator. Consequently, we also conclude that our numerical data below the deconfinement phase transition do not allow for an interpretation in terms of a quasi-particle picture. Above the deconfinement phase transition, on the other hand, we could fit the data by a physically motivated spectral function consisting of a quasiparticle branch and a plasmino branch with vanishing width, respectively. The obtained results for the current quark mass dependence of the thermal masses and for the dis-

person relations of quasiparticle and plasmino are then consistent with those from quenched lattice QCD. Furthermore we included a possible spacelike continuum contribution in the model spectral function which was not considered in the lattice calculations. We find this contribution to shift the dispersion relation of the plasmino into the timelike region. This indicates the importance of additional continuum contributions in the spectral function.

In addition we also analyzed our results by means of the so-called historical maximum entropy method. Although the method was shown to work for 'mock' data once the input was assumed to be accurate enough, the application to the numerical DSE results turned out to be more subtle. We interpreted the results as a hint that the spectral function, at least in the employed truncation, might not be positive semi-definite.

In summary, we conclude from this that we can achieve nice agreement with lattice QCD data in Euclidean space, but extracted spectral functions using fit forms should be taken with a grain of salt. Within the framework of Dyson-Schwinger equations this motivates future work of directly evaluating the spectral function. Although technically more evolved, calculations within models or using simpler truncations indicate that this is doable. Also the sensitivity on the gluon propagator and the quark-gluon vertex should be investigated, in particular since their analytic continuation to Minkowski space and therefore their spectral function is relevant for the outlined calculation. Furthermore it might be illustrative to analyze the lattice results of the gluon propagator along similar lines as has been done for the results of the quark propagator in quenched approximation.

### Acknowledgement

C. F. and J. M. were supported by the Helmholtz Young Investigator Grant VH-NG-332, by the Helmholtz Alliance HA216-TUD/EMMI and the Helmholtz International Center for FAIR within the LOEWE program of the State of Hesse. D.N. was supported by the German Research Foundation (DFG) under grant number Ni 1191/1-1 and by the DOE Office of Nuclear Physics under grant DE-FG02-00ER41132.

- 
- [1] B. Muller and J. L. Nagle, *Ann. Rev. Nucl. Part. Sci.* **56**, 93 (2006) [arXiv:nucl-th/0602029].
  - [2] E. Shuryak, *Prog. Part. Nucl. Phys.* **62**, 48 (2009) [arXiv:0807.3033 [hep-ph]].
  - [3] P. Braun-Munzinger and J. Wambach, *Rev. Mod. Phys.* **81**, 1031 (2009).
  - [4] U. W. Heinz, arXiv:0901.4355 [nucl-th].
  - [5] D. Molnar and S. A. Voloshin, *Phys. Rev. Lett.* **91**, 092301 (2003) [arXiv:nucl-th/0302014].
  - [6] R. Schulze, M. Bluhm and B. Kampfer, *Eur. Phys. J. ST* **155** (2008) 177 [arXiv:0709.2262 [hep-ph]]; M. Bluhm and B. Kampfer, *Phys. Rev. D* **77** (2008) 114016 [arXiv:0801.4147 [hep-ph]].
  - [7] W. Cassing, *Nucl. Phys. A* **791**, 365 (2007) [arXiv:0704.1410 [nucl-th]].
  - [8] W. Cassing and E. L. Bratkovskaya, *Phys. Rev. C* **78**, 034919 (2008) [arXiv:0808.0022 [hep-ph]].
  - [9] E. Braaten, R. D. Pisarski and T. C. Yuan, *Phys. Rev.*

- Lett. **64** (1990) 2242.
- [10] A. Peshier and M. H. Thoma, Phys. Rev. Lett. **84**, 841 (2000) [arXiv:hep-ph/9907268].
- [11] P. B. Arnold, G. D. Moore and L. G. Yaffe, JHEP **0206**, 030 (2002) [arXiv:hep-ph/0204343]; P. B. Arnold, G. D. Moore and L. G. Yaffe, JHEP **0112**, 009 (2001) [arXiv:hep-ph/0111107].
- [12] E. Braaten and R. D. Pisarski, Nucl. Phys. B **337** (1990) 569; E. Braaten and R. D. Pisarski, Phys. Rev. Lett. **64** (1990) 1338.
- [13] G. Baym, J. P. Blaizot and B. Svetitsky, Phys. Rev. D **46**, 4043 (1992).
- [14] J. P. Blaizot and J. Y. Ollitrault, Phys. Rev. D **48**, 1390 (1993) [arXiv:hep-th/9303070].
- [15] A. Schaefer and M. H. Thoma, Phys. Lett. B **451** (1999) 195 [arXiv:hep-ph/9811364].
- [16] M. Kitazawa, T. Kunihiro and Y. Nemoto, Phys. Lett. B **633** (2006) 269 [arXiv:hep-ph/0510167].
- [17] M. Kitazawa, T. Kunihiro and Y. Nemoto, Prog. Theor. Phys. **117** (2007) 103 [arXiv:hep-ph/0609164].
- [18] M. Harada, Y. Nemoto and S. Yoshimoto, Prog. Theor. Phys. **119**, 1 (2008) 117 [arXiv:0708.3351 [hep-ph]]; M. Harada and S. Yoshimoto, arXiv:0903.5495 [hep-ph].
- [19] W.H. Press, S.A. Teukolsky, W.T. Vetterling, and B.P. Flannery, *Numerical Recipes in C: The Art of Scientific Computing, Second Edition* (Cambridge University Press, Cambridge, 1992).
- [20] M. Jarrell and J. E. Gubernatis, Phys. Rep. **269** (1996) 133.
- [21] M. Asakawa, T. Hatsuda and Y. Nakahara, Prog. Part. Nucl. Phys. **46**, 459 (2001) [arXiv:hep-lat/0011040].
- [22] F. Karsch, E. Laermann, P. Petreczky, S. Stickan and I. Wetzorke, Phys. Lett. B **530**, 147 (2002) [arXiv:hep-lat/0110208]; S. Datta, F. Karsch, P. Petreczky and I. Wetzorke, Phys. Rev. D **69**, 094507 (2004) [arXiv:hep-lat/0312037].
- [23] D. Nickel, Annals Phys. **322** (2007) 1949 [arXiv:hep-ph/0607224].
- [24] F. Karsch and M. Kitazawa, Phys. Lett. B **658** (2007) 45 [arXiv:0708.0299 [hep-lat]].
- [25] F. Karsch and M. Kitazawa, Phys. Rev. D **80** (2009) 056001 [arXiv:0906.3941 [hep-lat]].
- [26] J. Braun, H. Gies, J. M. Pawłowski, Phys. Lett. **B684** (2010) 262-267. [arXiv:0708.2413 [hep-th]].
- [27] J. Braun, Eur. Phys. J. **C64** (2009) 459-482. [arXiv:0810.1727 [hep-ph]].
- [28] F. Marhauser, J. M. Pawłowski, [arXiv:0812.1144 [hep-ph]].
- [29] C. S. Fischer, Phys. Rev. Lett. **103** (2009) 052003 [arXiv:0904.2700 [hep-ph]].
- [30] C. S. Fischer and J. A. Mueller, Phys. Rev. D **80** (2009) 074029 [arXiv:0908.0007 [hep-ph]].
- [31] J. Braun, L. M. Haas, F. Marhauser and J. M. Pawłowski, arXiv:0908.0008 [hep-ph].
- [32] C. S. Fischer, A. Maas and J. A. Mueller, Eur. Phys. J. C **68**, 165 (2010) [arXiv:1003.1960 [hep-ph]].
- [33] A. Maas, J. Wambach, B. Grüter and R. Alkofer, Eur. Phys. J. C **37**, No.3, 335 (2004) [arXiv:hep-ph/0408074].
- [34] A. Maas, J. Wambach and R. Alkofer, Eur. Phys. J. C **42**, 93 (2005) [arXiv:hep-ph/0504019].
- [35] A. Cucchieri, A. Maas and T. Mendes, Phys. Rev. D **75**, 076003 (2007), [arXiv:hep-lat/0702022].
- [36] K. Lichtenegger and D. Zwanziger, Phys. Rev. D **78** (2008) 034038 [arXiv:0805.3804 [hep-ph]].
- [37] A. Kizilersu, D. B. Leinweber, J. I. Skullerud and A. G. Williams, Eur. Phys. J. C **50** (2007) 871 [arXiv:hep-lat/0610078].
- [38] R. Alkofer, C. S. Fischer, F. J. Llanes-Estrada and K. Schwenzer, Annals Phys. **324** (2009) 106 [arXiv:0804.3042 [hep-ph]].
- [39] M. Le Bellac, *Thermal Field Theory* (Cambridge University Press, Cambridge, 1996)
- [40] R. Alkofer, W. Detmold, C. S. Fischer and P. Maris, Phys. Rev. D **70** (2004) 014014 [arXiv:hep-ph/0309077]; Nucl. Phys. Proc. Suppl. **141** (2005) 122 [arXiv:hep-ph/0309078].
- [41] A. Bender, D. Blaschke, Y. Kalinovsky and C. D. Roberts, Phys. Rev. Lett. **77**, 3724 (1996) [arXiv:nucl-th/9606006].
- [42] C. Gattringer, Phys. Rev. Lett. **97** (2006) 032003 [arXiv:hep-lat/0605018]; E. Bilgici, F. Bruckmann, C. Gattringer and C. Hagen, Phys. Rev. D **77** (2008) 094007 [arXiv:0801.4051 [hep-lat]].